EUROGRAPHICS '97 / D. Fellner and L. Szirmay-Kalos
(Guest Editors)

Volume 16, (1997), Number 3

An Algorithmic Reflectance and Transmittance Model for Plant Tissue

Gladimir V. G. Baranoski and Jon G. Rokne

Department of Computer Science, The University of Calgary, Calgary, Alberta, Canada

Abstract

Recent developments in rendering have provided very realistic images. However, these images rarely show organic objects. We believe that one of the main difficulties of rendering these objects realistically is the lack of reflectance and transmittance models oriented to organic materials. In this paper an algorithmic reflectance and transmittance model for plant tissue oriented to computer graphics applications is presented. The model accounts for the three components of light propagation in plant tissues, namely surface reflectance, subsurface reflectance and transmittance, and mechanisms of light absorption by pigments present in these tissues. The model design is based on the available biological information, and it is controlled by a small number of biologically meaningful parameters. Its formulation, based on standard Monte Carlo techniques, guarantees its easy incorporation into most rendering systems. The spectral curves of reflectance and transmittance computed by the model are compared with measured curves from actual experiments.

Keywords: Physically-Based Rendering, Biologically-Based Rendering, BRDF, BTDF, BDF, Absorption.

1. Introduction

A substantial part of research in computer graphics is oriented towards image synthesis. In this context physically-based rendering plays an important role. Current research in this area focuses on ensuring the correctness of the results, which is directly associated with the *bidirectional surface-scattering distribution function* (BSSDF or simply BDF [44]) used to describe how the light interacts with different materials. The term BDF represents a combination of the BRDF (*bidirectional reflection distribution function*) and the BTDF (*bidirectional transmission distribution function*), which are used to describe the reflectance and transmittance characteristics of the materials.

Although many physically plausible BDF models (those whose existence does not violate the laws of physics [24]), have been proposed in the computer graphics literature [37], there is still a lack of models oriented to biological materials. In this paper we address this issue through the presentation of an algorithmic BDF model (ABM) that accounts for biological factors that affect light propagation and absorption in plant tissues. The model is oriented to leaves, since they are the most important plant surface interacting with light. However, it can easily be extended to other plant surfaces like petals and stems since they present similar optical and structural characteristics [6, 22].

Many researchers from areas like remote sensing and biology have proposed models for reflectance and transmittance for leaves where the goal is to understand physiological processes that relate foliar optical properties to biophysical characteristics [21]. For a comprehensive literature review in this area the reader is referred to the texts by Grant [12] and Vogelmann [40]. In realistic image synthesis we have different requirements, namely we are interested in incorporating the available biological information in a BDF model while keeping the cost/accuracy ratio low. Nonetheless some concepts used in those areas can be useful in computer graphics applications as well. For instance, some of the models developed by biologists and remote sensing researchers use the concept of layers, which is very intuitive, to simulate the light propagation in plant tissue [1, 20]. Recently computer graphics researchers, Hanrahan and Krueger [16], presented a model which simulates subsurface scattering using the concept of layered surfaces as well. Their model is oriented to a wide range of materials including organic tissue. However, in the

case of leaves, important biological factors affecting light absorption, reflection and transmission are not considered, and the predictions of their model are not compared to experimental data.

Many BDF models used in computer graphics rely on values of reflectance and transmittance either set by the user or obtained from the literature. Although spectral reflectance and transmittance curves are available for leaves [7, 13, 9], they are restricted to a narrow range of illuminating and viewing angles. Thus it becomes necessary to design a BDF model for plant tissue in which the reflectances and transmittances are calculated by the model itself. An exact model of a plant tissue would explicitly model individual cells. The model presented by Govaerts et al. [10, 11] is an example of such an approach. The drawbacks of such a model are that a large number of parameters are involved, which make the control difficult, and that a significant implementation overhead is required. Our strategy is to use a higher level of abstraction which allows our BDF model to be controlled by a small number of biologically meaningful parameters and enables its easy incorporation into most rendering systems. Its implementation is based on an algorithmic process through Monte Carlo methods [14]. Thus the BDF of a foliar tissue can be calculated and used on the fly during the rendering process, or computed and stored for validation purposes. We compare the results obtained using our model with the available experimental data [13, 9, 19, 3, 27, 42].

The remainder of this paper is organized as follows. The next section describes the foliar tissues and how they absorb and propagate light. Section 3 presents the algorithmic BDF model. Section 4 describes the testing procedures. Section 5 discusses the results and the performance issues. The paper closes with a summary and proposed extensions.

2. Foliar Tissues and the Propagation of Light

A leaf can be described as a diffusing and pigmented structure (mesophyll) having external plates of epidermal cells with a protective skin (cuticle). Figure 1a shows an idealized leaf cross-section. The outermost portion of the cuticle consists of epiticular wax. The surface roughness characteristics and the refraction index of the epiticular wax control the specularly reflected light from the adaxial (face) and abaxial (back) epidermis. No intercellular spaces are normally present in the epidermal tissues, and the cells usually fit one another like pieces of a jigsaw puzzle (Figure 1b). The mesophyll is composed of a densely packed layer of palisade cells, and a loosely packed layer of spongy cells. There are also species of plants which only have spongy mesophyll [41].

The palisade cells have a cylindrical shape, and 5 to 20% of their volume is air space. These cells present a high concentration of chloroplast which contain pigments, namely chlorophylls (mainly *a* and *b* forms) and carotenoids. The concentration and distribution of these pigments control the absorption of the light in the visible region of the light spectrum within the leaf. The spongy tissue consists of smaller cells, roughly ovoid to round in shape, that present less densely packed chloroplasts, with 50 to 80% of their volume occupied by air space [42]. The spaces between the mesophyll cells are also filled with air.

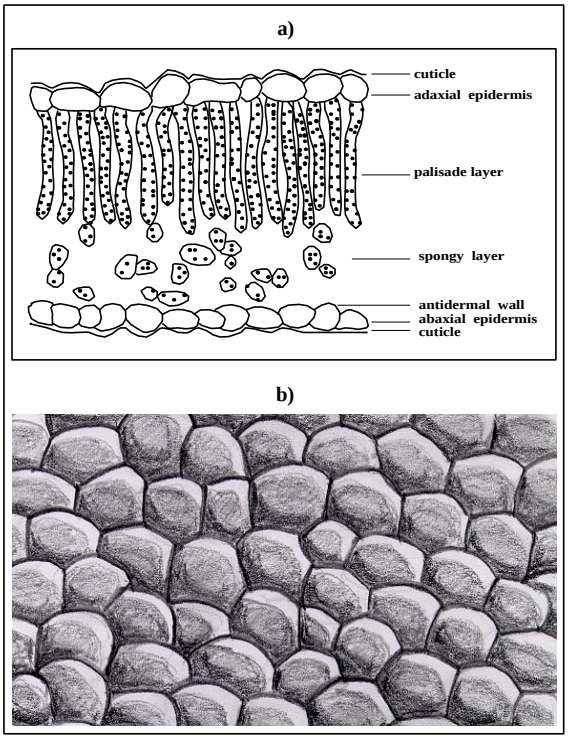

Figure 1: *a) Typical cross-section of foliar tissues. b) Artist's conception of a typical epidermis tissue (Courtesy of Daniel Dimian, The University of Calgary).*

Three principal types of scattering occur within the foliar tissues: Rayleigh, Mie and refractive-reflective scattering [39]. Rayleigh and Mie scatterings occur for particles of size equal to or less than the wavelength of the incident light respectively. In the case of the foliar tissues these particles correspond to organelles and macromolecules. Although the extent of and the exact causes of this forms of scattering in foliar tissues have not yet been completely resolved, their contribution to the total internal scattering is considered to be very low compared with the reflective-refractive scattering [39]. The dimensions of the palisade and spongy cells are quite large compared to the wavelength of the incident light, which make them responsible for this type of scattering. The reflective-refractive scattering accounts for most of the diffusion or internal scattering, and it is affected by the arrangement of tissues, and the refractive index differences, mainly air-cell wall interfaces.

Grant et al. [12, 13] describe leaves as having both specular and diffuse characteristics. The specular, non-Lambertian character of the leaf reflectance arises at the surface of the leaf. For some viewing directions, the surface reflection may be so large, that the leaves appear white instead of green. This happens when the white light visually overhelms the much smaller amounts of green light scattered by the interior of the leaves. The diffuse, Lambertian character of leaf reflectance emanates primarily from the mesophyll tissue through multiple scattering, with a small contribution of scattering from rough elements at the leaf surface. The multiple scattering in the leaf interior also gives the leaf transmittance a near-Lambertian distribution. In many species the adaxial epidermis is attached to the mesophyll over most of its inner surface (Figure 1a), so that once light past the outer epidermal surface, it can easily pass into the center of the leaf. The light entering or leaving the abaxial surface of a leaf, however, must pass through two semiplanar interfaces, namely air-abaxial epidermis and air-antidermal wall interfaces (Figure 1a). Thus light from a source on the back side of a leaf can penetrate the back epidermis and be reflected back by the inside surface of the epidermis without encountering the mesophyll. It is largely because of this factor that the leaf backs are often pale. The fact that the back surface of a leaf is a greater barrier to the escape of the oblique light than the face, explains why leaves that differ markedly in the structure of their two sides, show corresponding differences in their reflectance and transmittance curves.

3. The Algorithmic BDF Model

In the ABM light propagation is described in terms of ray optics, where light is assumed to be composed of non-interacting straight rays, each of them carrying a certain amount of energy [15]. The refractive-reflective scattering is assumed to be the dominant form of scattering within the foliar tissues. Instead of geometrically modeling many cells individually, the propagation of light within these tissues is simulated as a stochastic process whose states are associated with the air-cell wall interfaces represented in Figure 2. Once a ray hits a leaf it can be reflected at the state 1 (at interface 1) or state 4 (at interface 4) or refracted to the interior of the leaf. Then it can be reflected or refracted multiple times until it is absorbed at state 2 or leaves the leaf at the states 1 or 4.

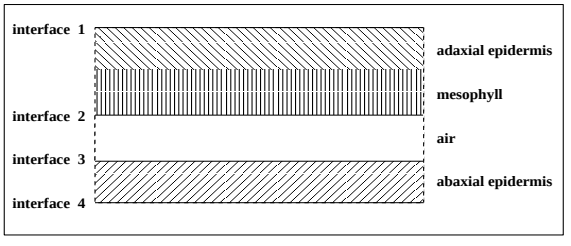

Figure 2: *Interfaces and tissues considered by ABM.*

The light interactions in our model may therefore be seen as a random walk [14] in which the transition probabilities are associated with the Fresnel coefficients (F) computed at each interface, and the termination probabilities are associated with the free path length (p) computed when a ray travels in the mesophyll layer towards or from interface 2. The Fresnel coefficients are computed through the Fresnel equations, which tell us the amount of light reflected and transmitted at an interface as a function of the incident light, the refractive index of the incidence medium (η_i), the refractive index of the transmission medium (η_t), the geometry of the surface and light, the angle of incidence (θ_i), and the angle of transmission (θ_t) given by the Snell's law:

$$\eta_i \sin\theta_i = \eta_t \sin\theta_t \tag{1}$$

A complete derivation of the Fresnel equations may be found in the texts by Hecht and Zajac [17] and Shirley [33]. Although they are valid only for infinite plane surfaces, in practice, as pointed out by Govaerts [10], these equations may still be used since a cell is large with respect to the wavelength of the incident light, and the portion of the cell wall interacting with a ray can be considered locally flat. Each time a ray hits an interface we compute the corresponding coefficient (F). We consider only the real parts of the refractive indexes, since for the spectral region covered in this work (400nm to 700nm), and for the materials considered, the complex parts are so small that they can be neglected. Then the equation used to compute the Fresnel coefficients at each interface, assuming unpolarized light [33], reduces to:

$$F = \frac{(\eta_i^2 - \eta_t^2)^2 c_{it}^2 + (\cos\theta_i^2 - \cos\theta_t^2)^2 n_{it}^2}{(c_{it}(\eta_i^2 + \eta_t^2) + n_{it}(\cos\theta_i^2 + \cos\theta_t^2))^2} \tag{2}$$

where:

$$c_{it} = \cos\theta_i \cos\theta_t$$
$$n_{it} = \eta_i \eta_t$$

After computing the Fresnel coefficient at an interface, we generate an uniform random number $\xi \in [0,1]$. If the random number ξ is smaller than or equal to the Fresnel coefficient F we generate a reflected ray $\vec{r}$, otherwise we generate a refracted ray $\vec{t}$. The reflected ray is obtained using the law of reflection in which the angle of the reflection direction, θ_r, is equal to the angle of the incidence direction, θ_i, and will be in the same plane as the incident ray $\vec{v}$ and a surface normal vector $\vec{n}$. The equation used is the following:

$$\vec{r} = \vec{v} + 2\vec{n}\cos\theta_i = \vec{v} - 2\vec{n}(\vec{v}\cdot\vec{n}) \tag{3}$$

The refracted ray is obtained using the Snell's law, as described by Heckbert [18], and is given by:

$$\vec{t} = \left[-\frac{\eta_i}{\eta_t} c_i - \sqrt{1 - \left(\frac{\eta_i}{\eta_t}\right)^2 (1 - c_i^2)} \right] \vec{n} + \frac{\eta_i}{\eta_t}\vec{v} \tag{4}$$

where:

$$c_i = \vec{v}\cdot\vec{n}$$

The ABM takes into account the three components of the plant tissues' BDF: surface reflectance, subsurface reflectance and transmittance. They are affected by the surface roughness, the light absorption in the mesophyll tissue, and the internal scattering. In the next sections we describe how we address these issues.

3.1. Scattering Profile

Brakke et al. [4] have noted that the scattering profile of a plant leaf can be approximated by an exponentiated cosine function. We have used a similar approach to simulate the distribution of the rays reflected or refracted at the foliar tissues. A rough surface, like a leaf epidermis, can contain more than one distinct scale of roughness. The contour of the epidermal walls represents large surface features with respect to the wavelength of the incident light. The microdetails of the epiticular waxes represent the small surface features relative to the wavelength of the incident light. For the plant epidermis, as pointed out by Grant [12] the large-scale roughness will dominate scattering in the specular direction, and the small-scale roughness will control scattering away from the specular direction. The epiticular waxes exhibit a wide range of geometric configurations, and their contribution to the overall reflectance is not as significant as the overall shape of the epidermal cells. For these reasons we have decided to concentrate our simulation efforts on the large scale features.

Govaerts et al. [11] have shown that the epidermal cells can be approximated by oblate ellipsoids. An oblate ellipsoid has semi-axes a_1, a_2 and a_3, and $a_1 = a_2$ but $a_3 < a_1$ [38]. For the plant cells we consider a_1 and a_2 as the axes in the plane of the foliar tissues, with values corresponding to average radius, a_r, of the cell. Unlike the oblateness definition used by Govaerts et al., we define the oblateness of the cell as $\frac{a_r}{a_3}$. The epidermal cells' dimensions regarding several species of plants can be found in the literature [45, 10, 26]. To simulate the effects of the epidermal cells' shape on the reflected rays at the air→epidermal cells interface, we perturb the rays using a warping function (5). This function corresponds to a PDF (probability density function [14]) based on an exponentiated cosine distribution [23], and the exponent is given by the epidermal cells' oblateness. The perturbation is performed through angular displacements, α_e and β_e. The angle α_e corresponds to the polar angle with respect to the ideal reflection or ideal transmission direction. The angle β_e corresponds to the azimutal angle around the ideal reflection or ideal transmission direction. These angles are given by:

$$(\alpha_e, \beta_e) = (\arccos[(1-\xi_1)^{\frac{1}{ob+1}}], 2\pi\xi_2) \qquad (5)$$

where:

ξ_1 and ξ_2 = uniform random numbers $\in [0,1]$.
ob = oblateness of the epidermal cells.

Therefore leaves whose epidermal cells' oblateness is large will have a surface reflectance closer to a specular distribution than leaves whose epidermal cells' oblateness is small.

When light passes to the mesophyll its direction of travel is randomized and it becomes diffuse. We simulate the distribution of the rays in this tissue using another warping function (6). In this case the PDF corresponds to a diffuse or cosine distribution [23]. The perturbation is also performed through angular displacements, α_m and β_m. The angle α_m corresponds to the polar angle with respect to the reflection or transmission direction of the propagated ray. The angle β_m corresponds to the azimutal angle around the propagation direction. These angles are given by:

$$(\alpha_m, \beta_m) = (\arccos(\sqrt{\xi_1}), 2\pi\xi_2) \qquad (6)$$

where:

ξ_1 and ξ_2 = uniform random numbers $\in [0,1]$.

Figure 3 presents a sketch showing the perturbations performed in each interface in both directions, upwards and downwards. In order to be consistent with available biological information and avoid undue complexity, we adopt a conservative strategy. In other words, we do not perturb the rays where the impact of the perturbation is not significant to the overall BDF.

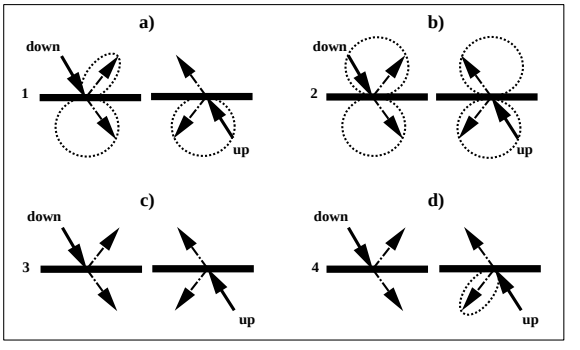

Figure 3: *Perturbations performed by ABM on the rays distributions at the four interfaces in the upwards and downwards directions of propagation considering the adaxial abaxial surface on the top and the abaxial surface on the bottom a) Interface 1. b) Interface 2. c) Interface 3. d) Interface 4.*

3.2. Absorption

A ray may encounter the mesophyll tissue after interacting with interface 1 or interface 2. Once it enters the mesophyll tissue it may be absorbed or propagated diffusively due to multiple interactions with the many air-cell walls' reflective-refractive discontinuities. When a perturbed refracted ray comes from interface 1 (Figure 4a), it is tested for absorption. If it is not absorbed the ray is tested for reflection or refraction at interface 2. If the outcome of the test is the refraction of the ray, it is perturbed and transmitted to interface 3. Otherwise the perturbed reflected ray (Figure 4b) is

tested for absorption. If it is not absorbed, it may be reflected back to the mesophyll at interface 1 (Figure 4c), restarting the mesophyll loop, or sending it back to the environment. When a ray comes from interface 3 it is also tested for reflection or refraction at interface 2. If the outcome of the test is a reflected ray, it is perturbed and sent it back to interface 3 without accounting for absorption. Otherwise, the refracted ray is perturbed (Figure 4d) and tested for absorption. If the ray is not absorbed, it proceeds in the mesophyll loop.

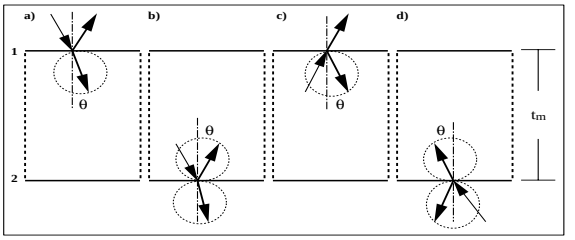

Figure 4: *Mesophyll loop. a) Ray coming from outside interacts with interface 1. b) Refracted ray from interface 1 interacts with interface 2. c) Reflected ray from interface 2 interacts with interface 1. d) Ray coming from interface 3 interacts with interface 2.*

The absorption of light in dye solutions varies with the thickness of the sample and the concentration of pigments in accordance with the Beer's law [1, 25]. It states that the transmissivity of a plate along its slant ray is given by:

$$T = \varepsilon^{-A\ c\ h\ \sec\theta} \tag{7}$$

where:
- A = specific absorption coefficient.
- c = concentration of pigment.
- h = thickness of plate.
- θ = angle of slant ray with respect to normal direction.

The absorption testing executed in state 2 of our model is based on Beer's law, and assuming a homogeneous distribution of pigments. It is performed probabilistically every time a ray starts a run in the mesophyll tissue. It consists of the estimated ray free path length, p, through the following expression:

$$p = -\frac{1}{A_g} ln(\xi) \cos\theta \tag{8}$$

where:
- ξ = uniform random number $\in [0, 1]$.
- A_g = global absorption coefficient of pigments.
- θ = angle between the ray direction and the normal direction.

The global absorption coefficient, as described by Jacquemoud and Baret [20], is given by:

$$A_g = \sum_{i=1}^{n} A_i\ c_i \tag{9}$$

where:
- A = specific absorption coefficient of a given pigment($\frac{cm^2}{\mu g}$).
- c = concentration of a given pigment (μg).

If p is greater than the thickness of the pigmented medium, t_m (both expressed in cm), then the ray is propagated, otherwise it is absorbed. The thickness value used in this comparison does not correspond to the total thickness of the leaf, but to a fraction of it. Since the palisade tissue presents a higher concentration of pigments than the spongy tissue, and it is largely responsible for the internal scattering, we suggest to use its length (around 45% of the total thickness) for most cases. For species that present an undifferentiated mesophyll tissue, e.g. characterized by the presence of spongy cells only [7, 41], we suggest using the entire length of the mesophyll tissue (around 75% of the thickness). The comprehensive set of leaf optical experiments, called *LOPEX* [19], provides the pigment concentrations and thickness values for leaf samples of more than fifty species. The curves for the specific absorption coefficient of chlorophyll and carotenoids pigments can be found in the paper by Jacquemoud and Baret [20]. Additional information on optical parameters of foliar tissues is available in a survey by Gausman and Allen [7].

3.3. Implementation Overview and Summary of Parameters

The model was implemented using the C^{++} language and the *ggLibrary* [36], a set of C^{++} utilities designed to be used in computer graphics applications. In the *ggLibrary* materials are classified as families, such as metals and dielectrics, and grouped by parameters that affect their behavior, following the ray tracing framework for global illumination proposed by Shirley et al. [35]. A set of routines specific for each family computes the BDF for that family. In the case of our model, the new family corresponds to the plant tissues, and the routines used to implement it correspond to each of the four states, which are called recursively by a controlling routine until the ray is either absorbed or leaves the material.

The parameters used in our model are the following:

- η_c - refractive index of the external cutinized wall of the epidermis: used in the Fresnel computations in states 1 and 4;
- *ob* - oblateness of epidermal cells: used in the perturbation of the rays in state 1 (Figure 3a), in state 3 (Figure 3c), and in state 4 (Figure 3d);
- η_m refractive index of the mesophyll cell wall: used in the Fresnel computations in state 2;
- t_m - thickness of mesophyll tissue: used in the absorption computation in state 2;

- c - concentration of pigments: also used in the absorption computations in state 2;
- η_a - refractive index of the antidermal wall: used in the Fresnel computations in state 3.

The refractive indexes come from experiments described in the literature [8, 20, 43]. The remaining parameters are also available in the literature, as mentioned earlier. The user may also adjust the optical parameters, e.g. t_m, depending on the conditions at hand. For example, for some species, a leaf in the sunlit and a leaf in the shady portions of a tree, may present differences of thickness of around 25% [2]. The curves for the specific absorption coefficient provided by Jacquemoud and Baret [20] and used in the absorption computations are independent of the plant species, since they refer to pigments commonly present in plant tissues. However, they may be adjusted according to the pigment concentration [28, 40]. Notice that we use the same parameters for the adaxial and abaxial epidermis. This approach is accurate for most cases, but for some species it may be more appropriate to use a set of parameters with slightly different values.

4. Testing Issues

One approach that comes to mind for validating a BDF model is visual inspection by comparing images generated using the model with images generated using previous models. This approach is not suitable in our case since the graphics literature lacks models oriented to plants. Validating our model in this manner is therefore not possible. Another alternative would be to compare the computer generated images using our model with photographs of real plants. In this case the validation of our model could be biased by error generated by other stages of the rendering pipeline, such as geometrical modeling, spectral modeling and directional sampling. Since our goal at this point of our research is not necessarily to generate the best possible image of a plant (but to contribute to its synthesis respecting the laws of physics), we chose, as a third alternative, to test our model as a separate unit of the rendering pipeline and compare the results with the best available experimental data.

In order to perform a comprehensive validation of a BDF model it would be necessary to consider all possible illuminating and viewing geometries. The very large number of measurements needed as well as the lack of experimental data covering all the possible instances precludes the use of this approach. Judd and Wyszecki [46] pointed out that in many goniophotometric measurements the most interesting and informative data for practical samples are taken in the plane given by the direction of the incident light and the normal of the specimen. Although the evaluation of a computer model is less predictable than measuring physical phenomena, we chose to use this plane in the testing of our model due to the practical reasons mentioned above.

4.1. Simulation of Photometric Devices

We are interested not only in the spectral curves of reflectance, ρ, and transmittance, τ, but also in the BRDF, f_r, and in the BTDF, f_t. The actual measurements of ρ and τ are performed using spectrophotometers equipped with an integrating sphere, and the actual measurements of f_r and f_t are performed using goniophotometers [46, 25]. In our simulation of a spectrophotometer with integrating sphere the rays are shot from an emitter placed above the specimen following an incident differential solid angle $d\vec{\omega}_i$. Considering a total number of N rays fired towards the specimen, one can assume that each ray carries the same amount of power Φ. If the total power to be shot is Φ^i, then, as stated by Shirley [33, 35], the power carried by each ray is given by:

$$\Phi = \frac{\Phi^i}{N} \tag{10}$$

Recall that reflectance describes the ratio of reflected power to incident power, and transmittance describes the ratio of transmitted power to incident power. Then if m_r rays are reflected towards the upper hemisphere, Ω_r, the spectral reflectance of the specimen with respect to a given wavelength λ of the incident light will be given by:

$$\rho(\lambda, d\vec{\omega}_i, \Omega_r) = \frac{m_r}{N} \tag{11}$$

The transmittance is calculated similarly considering the lower hemisphere.

In our simulation of a goniophotometer we use a slightly different arrangement. Instead of considering the entire upper and lower hemisphere as collectors, we use several detectors represented by the patches of a sphere placed around the specimen. Then if m_r rays hit a detector placed in the upper hemisphere, the BRDF with respect to a given wavelength λ of the incident light will be given by:

$$f_r(\lambda, d\vec{\omega}_i, d\vec{\omega}_r) = \frac{m_r}{N d\vec{\omega}_r{}^p} \tag{12}$$

where $d\vec{\omega}_r{}^p$ corresponds to the project solid angle regarding the reflectance detector. It is given by:

$$d\vec{\omega}_r{}^p = \frac{dA_r \cos\psi_r}{L^2} \tag{13}$$

where:

dA_r	=	differential area of the reflectance detector.
L	=	distance from the sample to the detector.
ψ_r	=	angle between the direction of reflectance and the specimen normal.

Similarly the BTDF is calculated considering detectors placed in the lower hemisphere.

The origins of the rays are random points uniformly chosen from a disk which corresponds to the emitter's surface. The coordinates of the points are given by the pair (Θ, l), which is computed using the following warping function

suggested by Shirley [33]:

$$(\Theta, l) = (2\pi\xi_1, R\sqrt{\xi_2}) \tag{14}$$

where:

ξ_1 and ξ_2 = uniform random numbers $\in [0,1]$.
R = radius of the disk.

The targets of the rays are random points uniformly chosen from a specimen represented by a pair of triangles. To choose a random point q on a triangle defined by the vertices q_0, q_1 and q_2 we use the following expression:

$$q = q_0 + \varphi(q_1 - q_0) + \gamma(q_2 - q_0) \tag{15}$$

where φ and γ are obtained using another warping function suggested by Shirley [33]:

$$(\varphi, \gamma) = (1 - \sqrt{1-\xi_1}, (1-\varphi)\xi_2) \tag{16}$$

where:

ξ_1 and ξ_2 = uniform random numbers $\in [0,1]$.

The precision of real photometric devices, as mentioned by Judd and Wyszecki [46], is measured by the ability of the instrument to repeat a measurement of a given specimen. For instance, a spectrophometer is considered to be of high precision if the spectral measurement, reflectance or transmittance, is repeated to a achieve a tolerance better than $\Delta(\lambda) = \pm 0.001$. In our simulations we select the number of rays N to be shot using this tolerance value to avoid undesirable fluctuations in the measurements.

4.2. Testing Parameters

LOPEX [19] is a set of leaf optical experiments recently performed on about 120 leaf samples representative of more than 50 species. The experiments include spectral curves of reflectance and transmittance as well as auxiliary measurements like pigment concentrations and thickness measurements. In order to compare our results with these measured values, we attempt to reproduce as faithfully as possible the actual measurement conditions. We use the same area for the specimen, 40mm^2, and the same angle of incidence, 8°, with respect to the normal of the specimen. Our emitter has a radius of 8mm, and it is positioned at a distance of 30mm from the center of the specimen. These values correspond to the area of the apertures and radius of the integrating sphere respectively.

η_c	1.6
ob	5.0
η_m	1.41
c	43.62
t_m	0.0072
η_a	1.42

Table 1: *Parameters used in the testing of ABM.*

We select, without loss of generality, a leaf from the soya species (*Glycine max, Soja hispida*), because of its standard foliar characteristics, and the large variety of experimental data available for comparison [9, 3, 42] besides *LOPEX*. The parameters used are presented in Table 1. The refractive indexes are provided by Wooley [43]. The oblateness was obtained using the average dimensions ($a_r = 12.5$, $a_3 = 2.5$) which are available in the texts by Govaerts et al. [11] and Norman [29]. The concentration of chlorophyll was obtained directly from *LOPEX*, and the thickness was computed using 45% of the total leaf thickness provided by *LOPEX* as proposed in section 3.2.

5. Results and Discussion

The spectral curves obtained from the model are qualitatively in agreement with the actual measured values (Figure 5). The quantitative discrepancies may be due to in part to the facts that we did not consider the carotenoids (which account for 20% of the total amount of pigments) and we did not separate different chlorophyll pigments. Moreover, the underestimation of surface microdetails, and shadowing and masking effects [5] may also contribute. Nevertheless it should be noted that Figure 5 represents mainly qualitative comparisons, between modeled and measured values, since some parameters used in the simulation, namely the refractive indexes and oblateness, correspond to average values published in the literature. Besides, as stated by Salisbury and Ross [32], the exact position of the absorption peaks depend on the solvents in which the pigments are dissolved, and one can expect small shifts considering *in vivo* values. For this reasons one must account for possible variations between the average values used by the model and the exact values regarding the leaf used in the actual measurements.

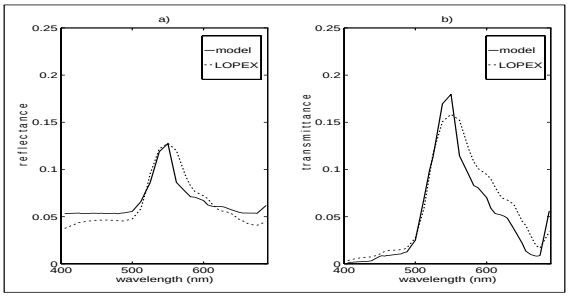

Figure 5: *Comparison of modeled spectral curves of a soybean leaf with measured spectral curves provided by LOPEX, for an angle of incidence of* 8° *and* 10^6 *rays. a) Reflectance curves. b) Transmittance curves.*

As pointed out by Vogelmann [40], the asymmetry in the leaf anatomy gives different reflectance and transmittance readings for the adaxial (face) and abaxial (back) surfaces. Spectrometric curves obtained experimentally by Wooley [42] show

greater reflectance for the backs than for the faces in the visible region of the spectrum. Figure 6a shows that our model can capture this aspect of foliar optics, which is responsible for the fact that the backs of most leaves appear pale to the eye. The experiments by Wooley also show greater transmittance when the leaf's back is toward the light, although in the visible region the differences of magnitude of the transmittances are not so high as the differences of magnitude of the reflectances. Figure 6b shows that our model can capture these characteristics of the transmittance curves as well.

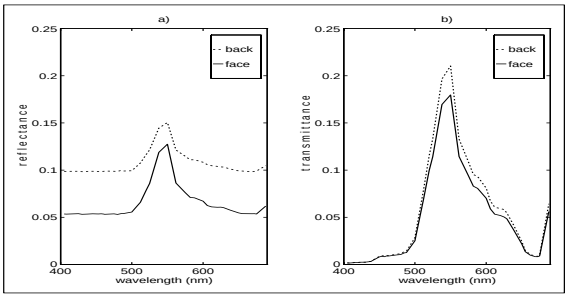

Figure 6: *Modeled spectral curves of a soybean leaf considering its face (adaxial surface) towards the light and its back (abaxial surface) towards the light, for an angle of incidence of* 8° *and* 10^6 *rays. a) Reflectance curves. b) Transmittance curves.*

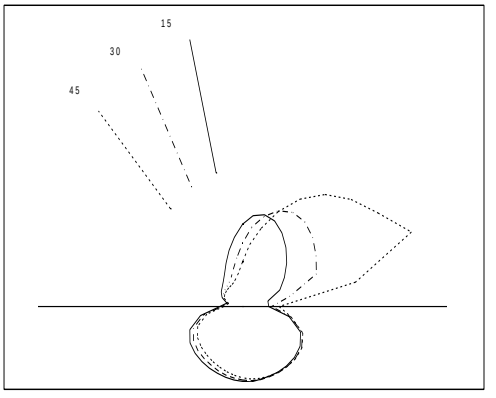

Figure 7: *BDF of a soybean leaf at a wavelength of* 550 *nm (which corresponds approximately to the reflectance and transmittance peaks), for angles of incidence of* 15°, 30° *and* 45°, *in the plane given by the incidence direction and the normal of the specimen,* 10^7 *rays, and the collector sphere divided into* 20 *patches along its latitude and* 40 *patches along its longitude.*

Figure 7 (upper part) shows that the simulated BRDF exhibits an angular dependency on the incident angle intermediate to that expected of diffuse and specular reflectors, which corresponds to the characteristics of the real BRDF of leaves [12]. It also shows (lower part) that the simulated BTDF has a near-Lambertian distribution, which is also a characteristic of the real BTDF of leaves [12]. Moreover the curves in Figure 7 generally agree with the experimental BDF curves published by Breece and Holmes [3] and Wooley [42].

Even though a performance analysis should in general not be based only on counting the number of interactions, since it does not account for differing amounts and types of work performed on each interaction, we believe that it may be illustrative of the behavior of our model. Figure 8 shows that, despite the stochastic nature of our model and the number of interfaces involved, the number of iterations (state transitions) is usually low. This suggests that the cost/accuracy ratio is compatible with physically-based rendering requirements. Furthermore in applications where the accuracy requirements for individual elements, such as a leaf or a petal, are not very high, e.g. the rendering of a tree with hundreds of leaves, the model may be reduced to its most important states, namely states 1 and 2.

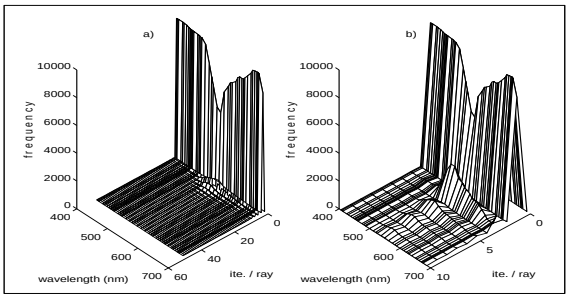

Figure 8: *Number of interactions per ray and per wavelength for* 10^4 *rays. a) Graph for zero to fifty interactions per ray, b) Zoom in of the region with high frequency of interactions per ray.*

The ABM is oriented to the visible region of the spectrum, but it may be adapted to be used in the applications regarding other regions, e.g. infrared applications [31]. Weights may be associated with the rays at each interaction accordingly with the Fresnel coefficient. In this case instead of tracking just one ray after each interaction, we would track two. This would represent additional implementation overhead, but it would reduce considerably the number of rays needed to satisfy the precision criteria. It would also allow the use of a *Russian roulette* procedure [44, 14] to stop the rays probabilistically in the 700-1300nm region which is characterized by the lack of absorption. In the 1300-2500nm region the absorption is controlled by the water content. For this region, in the absorption testing performed at state 2, one has to consider the absorption coefficients for water [30] instead of the absorption coefficients for pigments.

6. Conclusion and Future Research

In this paper we have presented a plausible BDF model for plant tissue that incorporates the biological information available. It can easily fit into most rendering systems since it is controlled by a small number of biologically meaningful parameters, and its formulation based on standard Monte Carlo methods provides adequation to efficient rendering techniques. Our simulations show good qualitative agreement with measured values while also showing that there is still room for improvement.

We intend to proceed with the investigation of the factors affecting the surface reflectance, and explore efficient alternatives to simulate the wax configurations, and shadowing and masking effects. We also intend to account for the presence of venation and hair, which affect the spectral curves as well. Although there is little experimental data on the anisotropy of plant tissues and the factors affecting it, this issue shall also be examined more closely.

Finally the complexity of the mechanisms involved in plant tissue optics makes selecting the "best" approach or the "best" model a delicate task. Developing practical solutions, including application of parallel processing techniques, will likely require a better understanding of the biological processes involved. We believe that this is a necessary step to increase the correctness and extend the range of applications of photorealistic rendering. Our future research efforts will be focused in this area.

Acknowledgments

We would like to thank Daniel Dimian for his helpful suggestions, Dr. Przemyslaw Prusinkiewicz for the fruitful discussions, and the anonymous reviewers for their useful insights. We are also grateful to the Joint Research Centre of the European Comission for granting us access to the *LOPEX* data set which was established during an experiment conducted by the Advanced Techniques Unit of the Space Applications Institute (Italy). The work presented in this paper was supported in part by CNPq (Proc. 200876/93-7, Brazil) and by NSERC (Grant 69-1266, Canada).

References

1. W.A. Allen, A.J. Richardson, and J.R. Thomas. Iteraction of isotropic light with a compact plant leaf. *Journal of the Optical Society of America*, 59(10):1376–1379, 1969.
2. W.A. Allen and A.J. Richardson. Willstater-stoll theory of leaf reflectance evaluated by ray tracing. *Applied Optics*, 12(10):2448–2453, 1973.
3. H.T. Breece III and R.A. Holmes. Bidirectional scattering characteristics of healthy green soybean and corn leaves in vivo. *Applied Optics*, 10(1):119–127, January 1971.
4. T.W. Brakke, J.A. Smith, and J.M. Harnden. Bidirectional scattering of light from tree leaves. *Remote Sensing of Environment*, 29:175–183, 1989.
5. A. Fournier. From local to global illumination and back. In *Rendering Techniques'95 (Proceedings of the Sixth Eurographics Rendering Workshop)*, pages 127–136, June 1995.
6. D.M. Gates, H.J. Keegan, J.C. Schelter, and V.R. Weidner. Spectral properties of plants. *Applied Optics*, 4(1):11–20, January 1965.
7. H.W. Gausman and W.A. Allen. Optical parameters of leaves of 30 plant species. *Plant Physiology*, 52:57–62, 1973.
8. H.W. Gausman, W.A. Allen, and D.E. Escobar. Refractive index of plant cell walls. *Applied Optics*, 13(1):109–11, 1973.
9. R.K. Gupta and J. T. Wooley. Spectral properties of soybean leaves. *Agronomy Journal*, 63:123–126, 1971.
10. Y. M. Govaerts. *A model of light scattering in three-dimensional plant canopies: a monte carlo ray tracing approach*. PhD thesis, Département of Physique, Faculté des Sciences, Université Catholique de Louvain-la-Neuve, 1995.
11. Y. M. Govaerts, S. Jacquemoud amd M. Verstraete, and S. L. Ustin. Three-dimensional radiation transfer modeling in a dycotyledon leaf. *Applied Optics*, 35(33):6585–6598, November 1996.
12. L. Grant. Diffuse and specular characteristics of leaf reflectance. *Remote Sensing of Environment*, 22:309–322, 1987.
13. L. Grant, C.S.T. Daughtry, and V.C. Vanderbilt. Polarized and specular reflectance variance with leaf surface features. *Physiologia Plantarum*, 88(1):1–9, 1993.
14. J.M. Hammerley and D.C. Handscomb. *Monte Carlo Methods*. Wiley, New York, N.Y., 1964.
15. R. Hall. *Illumination and Color in Computer Generated Imagery*. Springer-Verlag, New York, 1989.
16. P. Hanrahan and W. Krueger. Reflection from layered surfaces due to subsurface scattering. In *Proc. of SIGGRAPH*, pages 165–174, August 1993.
17. E Hecht and A. Zajac. *Optics*. Addison-Wesley, 1974.
18. P.S. Heckbert. *Writing a ray tracer*. Addison-Wesley, 1989.
19. B. Hosgood, S. Jacquemoud, G. Andreoli, J. Verdebout, G. Pedrini, and G. Schmuck. Leaf optical properties experiment 93. Technical Report Report EUR 16095 EN, Joint Research Center, European Comission, Institute for Remote Sensing Applications, 1995.

20. S. Jacquemoud and F. Baret. Prospect: A model of leaf optical properties spectra. *Remote Sensing of Environment*, 34(2):75–92, 1990.

21. S. Jacquemoud, S.L. Ustin, J. Verdebout, G. Schmuck, G. Andreoli, and B. Hosgood. Estimating leaf biochemistry using prospect leaf optical properties model. *Remote Sensing of Environment*, 56:194–202, 1996.

22. Q.O.N. Kay, H.S. Daoud, and C.H. Stirton. Pigment distribution, light reflection and cell structure in petals. *Botanic Journal of the Linnean Society*, 83:57–84, 1981.

23. E.P. Lafortune and Y. D. Willems. Using the modified phong reflectance model for physically based rendering. Technical report, Department of Computer Science, K.U. Leuven, November 1994.

24. R. R. Lewis. Making shaders more physically plausible. In *Proc. of the Fourth Eurographics Rendering Workshop*, pages 109–120, June 1993.

25. D.L. MacAdam. *Color Measurements Theme and Variations*. Springer Verlag, Berlin, 1981.

26. G. Martin, D.A. Myers, and T. Vogelmann. Characterization of plant epidermal lens effects by a surface replica technique. *Journal of Experimental Botany*, 42(238):581–587, May 1991.

27. J.H. McClendon. The micro-optics of leaves. i. patterns of reflection from the epidermis. *American Journal of Botany*, 71(10):1391–1397, 1984.

28. J.H. McClendon and L. Fukshansky. On the interaction of absorption spectra of leaves - ii. the non-absorbed ray of the sieve effect and the mean optical pathlength in the remainder of the leaf. *Photochemistry and Photobiology*, 51(2):211–216, 1990.

29. A.G. Norman. *Soybean Physiology, Agronomy, and Utilization*. Academic Press, New York, N.Y., 1978.

30. K. F. Palmer and D. Williams. Optical properties of water in the near infrared. *Journal of the Optical Society of America*, 64(8):1107–1110, August 1974.

31. Holly E. Rushmeier and Stephen D. Tynor. Incorporating the BRDF into an infrared scene generation system. In *Conference on Characterization, Propagation and Simulation of Infrared Scenes, SPIE Proceedings*, volume 1311, Orlando, Florida, April 1990.

32. F.B. Salisbury and C.W. Ross. *Plant Physiology*. Wadsworth Publishing Company, Belmont, California, 3 edition, 1985.

33. P. Shirley. *Physically based lighting for computer graphics*. PhD thesis, Dept. of Computer Science, University of Illinois, November 1990.

34. P. Shirley, K. Sung, and W. Brown. A ray tracing framework for global illumination systems. In *Graphics Interface'91*, pages 117–128. Canadian Information Processing Society, Toronto, 1991.

35. P. Shirley. Discrepancy as a quality measure for sample distributions. In F. H. Post and W. Barth, editors, *Proc. of the Annual Conference of the European Association for Computer Graphics - Eurographics'91*, pages 183–194, Amesterdam, 1991. North-Holland.

36. P. Shirley, G.V.G. Baranoski, B.S. Cho, A. Defrancesco, V. Gupta, B. Jones, R. Kamath, J. Kim, K. Kim, T. Loos, H. Ma, C. Meyer, D. Rusinov, S. Sampson, G. Vogl, B. Winnicka, K. Zimmerman, and S. Swamy. *The GG Library Reference Manual*. Indiana University, Bloomington, Indiana, 1993.

37. C. Schlick. An inexpensive BRDF model for physically-based rendering. *Proc. of the Annual Conference of the European Association for Computer Graphics - Eurographics'94*, 13(3):233–246, 1994.

38. L.L. Smail. *Analytic Geometry and Calculus*. Appleton-Century-Crofts, New York, N.Y., 1953.

39. C. J. Tucker and M.W. Garrat. Leaf optical system modeled as a stochastic process. *Applied Optics*, 16(3):635–642, 1977.

40. T.C. Vogelmann. Plant tissue optics. *Annual Review of Plant Physiology and Plant Molecular Biology*, 44:231–251, 1993.

41. T.C. Vogelmann and G. Martin. The functional significance of palisade tissue: penetration of directional versus diffuse light. *Plant, Cell and Environment*, 16:65–72, 1993.

42. J.T. Woolley. Reflectance and transmittance of light by leaves. *Plant Physiology*, 47:656–662, 1971.

43. J.T. Woolley. Refractive index of soybean leaf cell walls. *Plant Physiology*, 55:172–174, 1975.

44. A.S. Glassner. *Principles of Digital Image Synthesis*. Morgan Kaufmann, San Francisco, 1 edition, 1995.

45. R.A. Bone, D.W. Lee, and J.M. Norman. Epidermal cells functioning as lenses in leaves of tropical rainforest shade plants. *Applied Optics*, 24(10):1408–1412, May 1985.

46. D.B. Judd and G. Wyszecki. *Color in Business, Science and Industry*. John Wiley & Sons, New York, N.Y., third edition, 1975.